Astron. Astrophys. 337, 866–882 (1998)

ASTRONOMY AND ASTROPHYSICS

Galactic planetary nebulae with Wolf-Rayet nuclei

I. Objects with [WC]-early type stars⋆,⋆⋆

M. Peña[1⋆⋆⋆], **G. Stasińska**[2], **C. Esteban**[3], **L. Koesterke**[4], **S. Medina**[1], **and R. Kingsburgh**[5]

[1] Instituto de Astronomía, Universidad Nacional Autónoma de México, Apdo. Postal 70 264, México D.F. 04510, México (miriam@astroscu.unam.mx)
[2] DAEC, Observatoire de Paris-Meudon, F-92195 Meudon Cedex, (grazyna@obspm.fr)
[3] Instituto de Astrofísica de Canarias, Spain (cel@ll.iac.es)
[4] Lehrstuhl Astrophysik der Universitãt Potsdam, Germany (lars@astro.physik.uni-potsdam.de)
[5] Department of Physics and Astronomy, York University, Canada (robin@aries.phys.yorku.ca)

Received 25 February 1998 / Accepted 19 June 1998

Abstract. Spatially resolved long-slit spectrophotometric data for the planetary nebulae PB 6, NGC 2452, NGC 2867, NGC 6905 and He 2-55 are presented. Different knots were observed in each nebula. All the nebulae are ionized by [WC 2–3] type nuclei. For the five objects, we calculated photoionization models using the ionizing radiation field from models of expanding atmospheres. The photoionization models, built with the condition that the predicted stellar visual magnitude is equal to the observed one, were rather successful in reproducing at the same time the ionization structure and the electron temperature of the nebulae, using model atmospheres that were close ($\pm$20 000 K) to the best fit for reproducing the stellar features, as presented by Koesterke & Hamann (1997a). The constraints for the modelling procedure were to reproduce the observed intensity ratios of important lines of different ionization stages, and to be roughly consistent with the observed Hβ flux, angular diameter and morphology of the nebulae. We found that, for some objects, only two-density models with an inner zone of lower density can meet all these requirements. These density structures are consistent with the morphology showed by the nebulae. In a couple of cases, our photoionization modelling seems to indicate that the models of expanding atmospheres used could be lacking ionizing photons with respect to their emission in the V band.

Chemical abundances in the nebulae were derived from the ionic abundances observed and ionization correction factors obtained from the models. We found that, while the five nebulae of our program have very similar exciting stars (similar stellar temperatures, mass loss rates, chemical compositions), the nebular chemical compositions are different. PB 6 and NGC 2452 are He-, N-, and probably C-rich nebulae, indicating massive progenitors ($M_{\rm initial} \geq 2.8 M_{\odot}$). In particular, abundances in PB 6 are consistent with a scenario of C produced via the triple-α process, being brought to the surface by the third dredge-up event and partially converted into N through envelope-burning. The other nebulae present typical disk-PNe abundances, showing only C enrichment (C/O $\geq$ 1). Therefore their progenitors were not massive, but all underwent the third dredge-up. Thus, clearly, post-AGB stars of quite different initial masses can pass through a [WC] stage with similar atmospheric parameters. We did not find evidence for abundance variations inside any of the nebulae. In PB 6 and NGC 2867, we found that the C/O ratios derived from the C III] 1909/[O III] 5007 line ratios would induce electron temperatures significantly lower than observed. The discrepancy would be larger if carbon abundances derived from the optical C II 4267 recombination lines are considered.

Key words: planetary nebulae: general – ISM: abundances – stars: Wolf-Rayet

1. Introduction

Only about 50 planetary nebulae (PNe) in our Galaxy have central stars with detected WR features (WRPNe) among 350 PNe with a stellar continuum measured and over 1000 PNe with nebular spectroscopy available (Tylenda et al. 1993). All these objects have been reported to have WC-type central stars, mostly of [WC 2–4] and [WC 8–11] spectral types, with very few objects in the intermediate classes (Tylenda et al. 1993). This distribution among [WR] types is very different from the one found for Population I WR stars. The latter are divided into WN and WC types, and, among the WC types, stars are distributed preferentially in the intermediate classes with a few objects in the late and early types. While many studies have been devoted, with undeniable success, to the genesis and evolution of Population I WR stars (e.g., Meynet 1995 and references therein), the evolutionary status of the [WR] central stars of PNe is unknown. It is

Send offprint requests to: M. Peña

⋆ Partially based on data obtained at the Observatorio Astronómico Nacional, SPM, B.C., México

⋆⋆ Figs. 5a to 5e are only available in the electronic version of the paper

⋆⋆⋆ Visiting astronomer at Cerro Tololo Inter-American Observatory operated by AURA under contract with the NSF.

Table 1. General properties of the studied objects and sources of the UV data.

	Central star				Diam.	Log total	
Object (PN G)	$m_V^{(1)}$	Spec. type$^{(2)}$	$T_*^{(2)}$(kK)	$R_t^{(2)}$($R_\odot$)	($''$)	$I(H\beta)^{(3)}$	source of *UV* data
PB 6 (278.8+4.9)	16.5	[WC 2]	141	4.50	12	−11.44	Henry et al. 1996
NGC 2452 (243.3−01.0)	17.0	[WC 2]	141	3.98	19	−10.94	Kingsburgh & Barlow 1994
NGC 2867 (278.1−05.9)	15.5	[WC 2]	141	3.98	14	−10.23	Kingsburgh & Barlow 1994
NGC 6905 (061.4−09.5)	15.5	[WC 2-3]	141	3.41	24$^{(4)}$	−10.69	Johnson 1981
He 2-55 (286.3+02.8)	16.3	[WC 3]	128	5.20	18	−11.95	Feibelman 1995

[1] Dereddened magnitudes derived from the stellar flux at 5480 Å.
[2] Stellar types, temperature and transformed radius as given by Koesterke & Hamann (1997a).
[3] Total Hβ fluxes from Acker et al. (1992), corrected for extinction.
[4] Diameter of the bright disk of the nebula.

not understood how a central star can expose its hydrogen-free layers before a temperature of 100 000 K is reached and how its atmosphere can be as carbon-rich as observed (Schönberner & Blöcker 1996), nor is it quite clear whether the [WC] types from 11 to 2 represent an evolutionary sequence, as suggested by Hamann (1997).

One may expect that a detailed study of the nebulae themselves will cast some light on our understanding of the history of these stars. So far, globally, WRPNe have not shown any significant difference relative to the PNe with non WR-type central stars, except larger expansion velocities (Górny & Stasińska 1995). Recent studies of the WRPNe in the Magellanic Clouds (Peña et al. 1997a) have arrived at the same conclusion, namely that WRPNe do not show significant differences when compared with non WR-type PNe. However, a more detailed spectroscopic study might reveal chemical inhomogeneities due to the presence of material processed by the central stars, like in the case of the knots in A 30 and A 78 (Jacoby & Ford 1983). This is one of the aims of the present study.

Searching for abundance variations across the face of a nebula requires good-quality spatially resolved spectra, together with a reliable procedure to correct for the unseen ions. Such a procedure is best achieved by constructing photoionization models that reproduce satisfactorily the main observed properties of each individual object under study.

In the recent years, a great effort has been devoted to compute models of expanding atmospheres for WR-type central stars. These models have been successfully applied to early and late [WC]-type nuclei in order to derive the fundamental stellar parameters (e.g., Leuenhagen et al. 1997; Koesterke & Hamann 1997a, b; De Marco & Crowther 1998). It is thus possible to use the ionizing radiation field predicted by these models to compute the ionization and thermal structure of WRPNe.

We have started a program of systematic observations of WRPNe to obtain spatially resolved spectroscopic data of the nebulae and their nuclei. In this work, we present the results concerning five objects which are excited by [WC 2–3] type stars. These are: PB 6 (PN G 278.8+4.9), NGC 2452 (PN G 243.3−01.0), NGC 2867 (PN G 278.1−05.9), NGC 6905 (PN G 061.4−09.5), and He 2-55 (PN G 286.3+02.8). According to models of expanding atmospheres that have been calculated to fit the observed stellar features (Koesterke & Hamann 1997a), these stars show very similar atmospheric characteristics, presenting similar temperatures, chemical compositions and wind parameters. On the other hand, the nebulae display important differences.

General properties of the central stars and nebulae are presented in Table 1. In this table, the stellar magnitudes listed were derived from the dereddened stellar continuum fluxes at 5480 Å measured in our spectra (after subtracting the nebular continuum). The uncertainties in these measurements are about $\pm$0.2 mag considering that a small fraction of the light could have escaped from the narrow slit. Our values are in very good agreement with the stellar magnitudes reported by Acker et al. (1992).

The spectral classification of the stars is based on the classification scheme by Méndez & Niemela (1982) which takes into account the relative strength of the optical C IV 5805 and C III 5695 lines and the O V 5598 , O VI 5290 and O VII 5670 lines. In all our stars, the C IV 5808 doublet has an equivalent width larger than 20 Å, but the most prominent emission feature is the huge O VI 3811-34 blend (see Fig. 2). Consequently, according to the recent classification scheme proposed by Crowther et al. (1998a) these central stars could be also classified as early [WO] type stars. Crowther et al. (1998a) indeed classified PB 6 and NGC 6905 as [WO 1] stars.

In this work we analyze long-slit optical spectrophotometric data combined with *UV* data from the *IUE* archives or from the literature to cover a wide wavelength range and to include the important *UV* carbon lines. In Sect. 2 the optical and *UV* data for the nebulae are presented, and we derive the usual plasma diagnostics (electron temperatures and densities). In Sect. 3, we describe the general approach used to model the nebulae. The chemical abundances found for each object on the various lines of sight are presented in Sect. 4. In Sect. 5, each object is discussed individually and the main conclusions are summarized in Sect. 6.

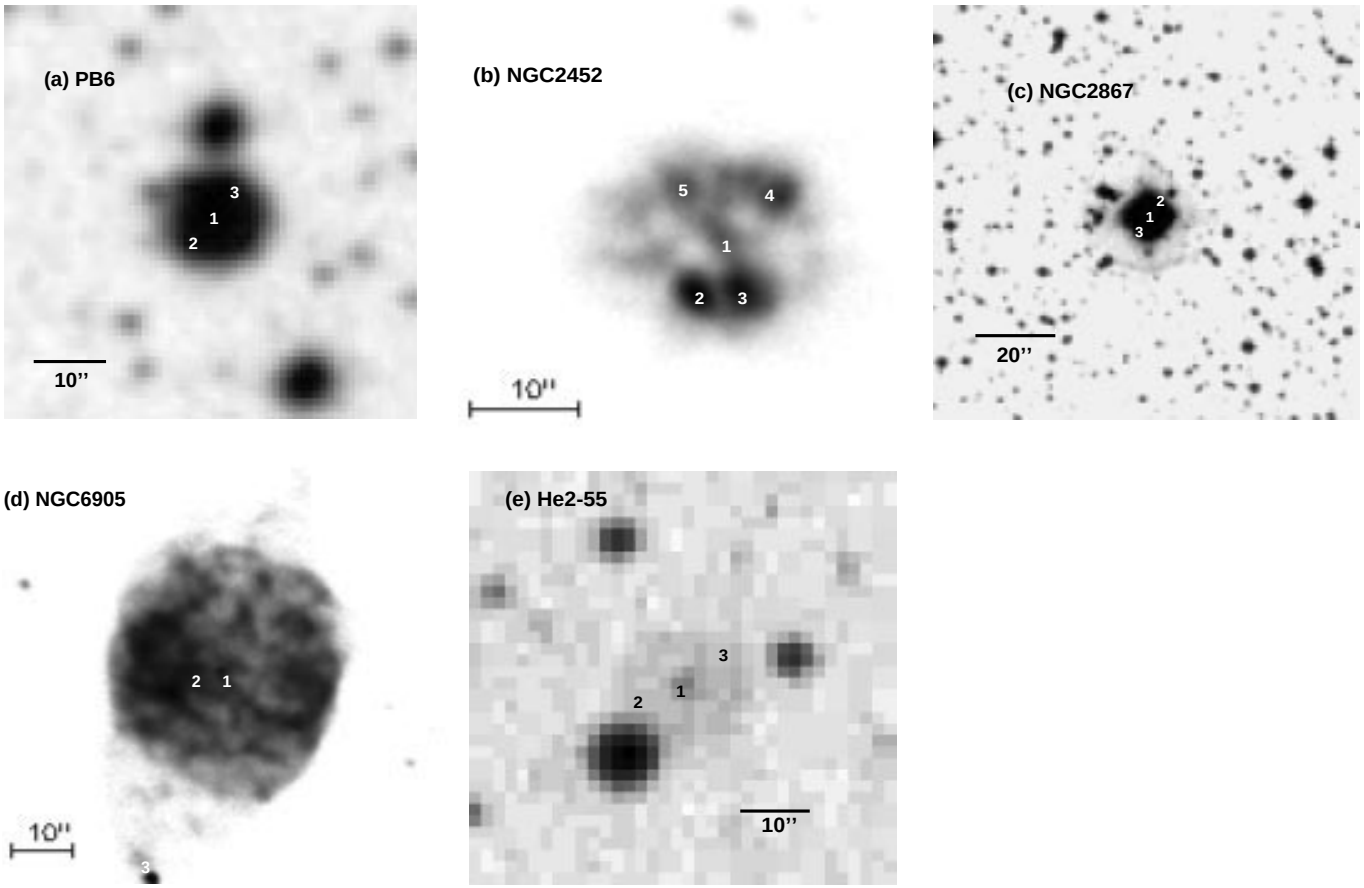

Fig. 1. Direct images of the studied nebulae, with the analyzed positions (as numbered in Tables 3 and 4) indicated on them. PB 6 and He 2-55 were obtained from the Palomar Observatory DSS; NGC 2452, and NGC 6905, from Balick (1989) and NGC 2867, from Schwarz et al. (1992)

2. Observational data and plasma diagnostics

2.1. Optical observations

Long-slit spectrophotometric data for PB 6, He 2-55, NGC 2452 and NGC 2867 were obtained at CTIO, on 1994 December 29 and 30. The 4-m telescope, equipped with a RCS spectrograph, a Reticon detector (1200×400 pix) and the grating KPGL#2, was employed. Observations were performed under photometric conditions, allowing to obtain a spatial resolution better than $2''$ along the slit.

Several spectra with slit widths of $2''$ at different slit orientations were acquired for each object, trying to observe interesting knots in the nebulae. The wavelength range from 3170 to 7470 Å was covered with a resolution of 5-6 Å. In all the cases the slit was centered in the central star and rotated along the different position angles. The log of optical observations is described in Table 2.

NGC 6905 was observed in 1995 July 30 and 1996 June 15, at the Observatorio Astronómico Nacional, San Pedro Mártir, B.C., México, with the 2.1-m telescope and the REOSC *echelle* spectrograph in the high resolution mode. The spectral range observed was 3600-6700 Å with a spectral resolution of about 0.5 Å and a spatial resolution of about $1''.5$. Three different zones, described in Table 2, were observed.

Table 2. Log of CTIO and OAN observations.

Object	P.A.	Exp. time (s)	Comments
PB 6	135°	120	CTIO, 3 spectra CS+knots
NGC 2452	152°	300	CTIO, 2 spectra CS+knots
”	195°	300	CTIO, 2 spectra CS+knots
NGC 2867	150°	180, 60, 15	CTIO, 3 spectra CS+knots
”	70°	10	CTIO, 6 spectra CS+knots
NGC 6905	E-W	900	OAN, 2 spectra CS position
”	N-S	900	OAN, 2 spectra, $5''$ north from CS
”	E-W	900	OAN, 3 spectra of southern ansa
He 2-55	135°	300	CTIO, 2 spectra CS+knots

Spectrophotometric standard stars from the list by Hamuy et al. (1992) were observed in both sets of observations for flux calibration. Data reduction was performed at Cerro Calán Observatory, University of Chile, and Instituto de Astronomía, UNAM, using the IRAF[1] reduction package.

Fig. 1 shows direct images of PB 6, NGC 2452, NGC 2867, NGC 6905 and He 2-55 with the studied positions, as numbered

[1] IRAF is distributed by NOAO, which is operated by AURA, Inc., under contract with the NSF.

Table 3a. Dereddened fluxes for PB 6

	pos. 1(CS)	pos. 2	pos. 3
$\Theta^{(1)}$	0.″0	4.″4	4.″4
extraction ap.	$2'' \times 5''$	$2'' \times 5''$	$2'' \times 8''$
He I 5876	0.050	0.085	0.084
He II 1640	10.40	...	...
He II 4686	1.48	1.19	1.20
[O I] 6300	0.040	0.066	0.044
[O II] 3726+29	0.68	1.02	0.80
[O II] 7320+30	0.058	0.087	0.047
O III] 1663	0.43	...	...
[O III] 4363	0.183	0.19	0.18
[O III] 5007	9.71	10.99	11.31
O IV] 1402	0.82	...	...
C II] 2323	...	...	...
C II 4267	0.006:	...	...
C III] 1909	12	...	...
C IV 1549	16	...	...
[N I] 5200	0.016	0.036	0.023
[N II] 5755	0.041	0.058	0.046
[N II] 6584	2.07	3.29	2.38
N III] 1750	1.0	...	...
N IV] 1485	3.1	...	...
N V 1240	2.1	...	...
[Ne III]3869	1.10	1.21	1.22
[Ne IV] 2423	...	...	...
[Ne IV] 4725	0.023	0.025	0.024
[Ne V] 3426	1.44	0.58	0.60
[S II] 4069	0.039	0.044	0.038
[S II] 6717	0.048	0.085	0.060
[S II] 6731	0.071	0.110	0.079
[S III] 6312	0.035	0.030	0.032
[Ar III] 7136	0.151	0.171	0.163
[Ar IV] 4711	0.239	0.100	0.101
[Ar IV] 4740	0.108	0.072	0.075
[Ar V 7006	0.047	0.033	0.030
Δ Balmer /Hβ	...	3.9-03	4.1-03
c(Hβ)	0.42	0.53	0.34
t[O III]$^{(2)}$	1.48±0.06	1.43±0.06	1.37±0.06
t[N II]$^{(2)}$	1.13±0.08	1.09±0.08	1.14±0.08
t[O II]$^{(2)}$	1.3±0.2	1.7±0.2	1.2±0.2
t(Δ Balmer)$^{(2)}$	...	1.46±0.09	1.35±0.08
N_e[S II]$^{(2)}$	2.7±0.5	1.7±0.6	1.7±0.6
N_e[Ar IV]$^{(2)}$	0.01::	0.2::	0.08::

(1) Θ is the angular distance from the central star

(2) In all the tables t is in 10^4 K and N_e, in 10^3 cm^{-3}

in Tables 3 and 4, indicated on them. For the objects observed at CTIO (all but NGC 6905), the long slit was centered in the central star and spectra from the central position and from the knots at both sides of the star were extracted. The position angles used (P.A.) are indicated in Table 1 and the extraction apertures for each position are presented in Tables 3a-e.

Calibrated spectra of the central zones for the five objects are shown in Fig. 2. The spectrum of NGC 6905 consists of 30 orders of the *echelle* spectra joined together; notice that the spectral resolution is much higher and the flux scale is different for this object.

The nebular emission lines were measured in all the spectra. The observed fluxes were corrected for reddening according to the expression:

$$\log I(\lambda) \,/\, I(\mathrm{H}\beta) = \log F(\lambda) \,/\, F(\mathrm{H}\beta) + c(\mathrm{H}\beta) \times f_\lambda \ , \quad (1)$$

where $I(\lambda)$ and $F(\lambda)$ are the dereddened and observed fluxes respectively, $c(\mathrm{H}\beta)$ is the logarithmic reddening correction at Hβ, and f_λ is the reddening law. For both, the visual and *UV* regions, we employed the reddening law by Seaton (1979). The value of $c(\mathrm{H}\beta)$ was derived for each object from the Balmer decrement, by considering case B recombination theory (Hummer & Storey 1987). The most important lines, relative to Hβ and corrected for reddening, are presented in Tables 3a-e, where we also present the values of $c(\mathrm{H}\beta)$ for each position.

We estimate that, for the objects observed at CTIO, the line intensities are generally accurate within 5% for lines with $I(\lambda)/I(\mathrm{H}\beta) > 1$, 10% for lines with $I(\lambda)/I(\mathrm{H}\beta) \sim 0.1$ and 15% for lines with $I(\lambda)/I(\mathrm{H}\beta) \sim 0.01$. For NGC 6905, which was observed at San Pedro Mártir, the uncertainties are probably twice as high. The data marked with a colon have uncertainties larger than 50%.

2.2. UV data

UV spectroscopic data were obtained from the literature and/or extracted from *IUE* archives. In Table 1 we list the references for these data. We have chosen *IUE* low-dispersion (spectral resolution of 6-7 Å), large-aperture ($10'' \times 23''$) observations to extract the data. In principle, this means that the dereddened *UV* line fluxes (scaled to the optical observations and relative to Hβ) represent an average over a large fraction of the nebula. However, very often, in the raw images, only the brightest central region of the nebula stands out above the noise, so it is not clear to which region the *UV* line intensities actually pertain. We will assume that *IUE* data is representative of the central zone of the nebula.

Dereddened *UV* line intensities, relative to Hβ, are presented in Tables 3a-e, together with the optical data. We estimate that even for the most intense lines, when the flux can be measured with a good precision, the line intensities relative to Hβ are not more accurate than 30%. The large uncertainty is a consequence of the importance of the reddening corrections for the *UV* lines and of the difficulty to match the optical and *UV* data, which are obtained with very different apertures. This process is complex, because it depends on the ionization structure of the nebula and on its surface brightness distribution. In the case of our objects, an additional source of uncertainty is the fact that, most of the times, the differences in aperture between the optical and *IUE* data is corrected using the nebular He II 1640/4686 theoretical ratio, which in the case of WRPNe could be contaminated by stellar emission.

Table 3b. Dereddened fluxes for NGC 2452

	pos. 1 CS	pos. 2	pos. 3	pos. 4	
$\Theta^{(1)}$	0″	6″	8″	5″	9″
extraction ap.	2″ × 5.″3	2″ × 7″	2″ × 8.″8	2″ × 5.″3	2″ × 5.″3
He I 5876	0.078	0.103	0.109	0.084	0.081
He II 1640	5.63	...	...	...	...
He II 4686	0.759	0.611	0.527	0.655	0.743
[O I] 6300	0.047	0.129	0.115	0.052	0.033
[O II]3727+29	0.74	1.42	1.59	1.02	0.802
[O II]7320+30	0.045	0.105	0.084	0.049	0.033
O III] 1663	...	...	...	...	...
[O III] 4363	0.158	0.132	0.122	0.136	0.134
[O III] 5007	11.6	12.5	11.8	12.7	13.0
C II 4267	0.006:	...	...	...	...
C III] 1909	4.2	...	...	...	...
C IV 1549	3.1	...	...	...	...
[N I] 5200	0.012	0.030	0.032	0.014	0.065
[N II] 5755	0.015	0.038	0.037	0.021	0.014
[N II] 6584	1.12	2.47	2.44	1.38	1.07
N III] 1750	0.6	...	...	...	...
N IV] 1485	0.9	...	...	...	...
N V 1240	...	...	...	...	...
[Ne III] 3869	1.05	1.29	1.23	1.15	1.07
[Ne IV] 2423	1.4	...	...	...	...
[Ne IV] 4725	0.004:	0.006	...	...	...
[Ne V] 3426	0.654	0.222	0.138	0.19	0.21
[S II] 4069	0.042	0.065	0.057	0.045	0.040
[S II] 6717	0.114	0.247	0.254	0.148	0.111
[S II] 6731	0.146	0.322	0.304	0.191	0.140
[S III] 6312	0.040	0.052	0.044	0.046	0.040
[Ar III] 7136	0.264	0.365	0.321	0.309	0.277
[Ar IV] 4711	0.059	0.074	0.065	0.080	0.075
[Ar IV] 4741	0.053	0.059	0.050	0.063	0.060
[Ar V] 7006	0.021	0.016	0.007	0.011	0.013
Δ Balmer /Hβ	...	4.1-03	4.3-03	4.2-03	4.3-03
c(Hβ)	0.42	0.55	0.52	0.55	0.58
t[O III]	1.29±0.06	1.19±0.07	1.17±0.08	1.18±0.07	1.17±0.08
t[N II]	0.97±0.07	1.03±0.07	1.03±0.07	1.03±0.08	1.03±0.08
t[O II]	1.3±0.1	1.5±0.1	1.2±0.1	1.1±0.1	1.01±0.09
t(Δ Balmer)	...	1.15±0.09	1.06±0.09	1.13±0.10	1.11±0.10
N_e[S II]	1.59±0.50	1.6±0.5	1.2±0.7	1.5±0.5	1.4±0.6
N_e[Ar IV]	2.4±0.8	1.1±0.8	0.8±0.5	1.0±0.5	1.1±0.5

(1) Θ is the angular distance from the central star

2.3. Plasma diagnostics

The wide wavelength range observed allowed us to perform a complete plasma diagnosis. All the available diagnostic line ratios were analyzed. Electron temperatures were derived from [O III] 4363/5007, [N II] 5755/6583, [S II] 4069/6725 and [O II] 3727/7325 line intensity ratios and from the H I Balmer-discontinuity flux difference relative to $I(\mathrm{H}\beta)$ (taking into account the He^{+} and He^{++} contribution). Electron densities were derived from the [S II] 6717/6731 and [Ar IV] 4711/4740 line ratios. The results are presented, separately for each object, at the bottom of Tables 3a-e.

For PB 6, NGC 2452 and NGC 2867, the Balmer-discontinuity temperatures are very accurate with uncertainties of about 1 000 K. We note that for these objects, the Balmer discontinuity temperatures are equal, within the uncertainties, to the temperature derived from the [O III] 4363/5007 ratio; therefore, at least in these objects, there is no suspicion that large

Table 3c. Dereddened fluxes for NGC 2867.

	pos. 1: CS	pos. 2	pos. 3
$\Theta^{(1)}$	0″	4″	4″
extraction ap.	2″ × 5.″6	2″ × 5.″6	2″ × 6″
He I 5876	0.106	0.130	0.131
He II 1640	2.9	...	...
He II 4686	0.425	0.247	...
[O I] 6300	0.04	0.11	0.09
[O II] 3726+29	0.785	1.21	1.28
[O II] 7320+30	0.079	0.112	0.109
O III] 1663	0.21	...	...
[O III] 4363	0.143	0.141	0.132
[O III] 5007	13.6	12.9	13.6
O IV] 1402	0.07:	...	...
C II] 2323	0.87	...	...
C II 4267	0.010	0.011	...
C III] 1909	9.5	...	...
C IV 1549	2.8	...	...
[N I] 5200	0.008	0.009	0.008
[N II] 5755	0.009	0.019	0.015
[N II] 6584	0.460	0.803	0.720
N III] 1750	0.1:	...	...
N IV] 1485	0.2:	...	...
N V 1240	...	...	...
[Ne III] 3869	1.10	1.03	1.26
[Ne IV] 2423	0.35	...	...
[Ne IV] 4725	0.003:	...	...
[Ne V] 3426	0.049	0.009	0.025
[S II] 4069	0.026	0.034	0.031
[S II] 6717	0.039	0.055	0.059
[S II] 6731	0.058	0.082	0.089
[S III] 6312	0.020	0.018	0.018
[Ar III] 7136	0.071	0.108	0.149
[Ar IV] 4711	0.052	0.030	0.
[Ar IV] 4740	0.026	0.021	...
[Ar V] 7006	...	...	...
Δ Balmer /Hβ	...	4.1-03	4.3-03
c(Hβ)	0.35	0.35	0.37
t[O III]	1.17±0.06	1.18±0.06	1.14±0.06
t[N II]	1.12±0.10	1.20±0.09	1.16±0.09
t[O II]	1.5±0.3	1.4±0.2	1.3±0.2
t(Δ Balmer)	...	1.07±0.10	0.97±0.10
N_e[S II]	2.7±0.5	2.5±0.5	2.7±0.5
N_e[Ar IV]	0.01::	0.01::	1.0±0.7

(1) Θ is the angular distance from the central star

Table 3d. Dereddened fluxes for NGC 6905

	pos.1 CS	pos.2	pos.3 (ansa)
$\Theta^{(1)}$	0″	5″ E	20″ S
extraction ap.	2″ × 5″	2″ × 5″	2″ × 4″
He I 5876	0.04	0.026	0.09
He II 1640	5.9	...	...
He II 4686	0.83	1.01	0.62
[O I] 6300	0.018	0.019	0.20
[O II] 3727	0.162	0.123	4.28
[O II] 7325	0.060(2)	...	...
O III] 1663	0.7::	...	...
[O III] 4363	0.105	0.104	0.20
[O III] 5007	9.22	7.44	12.6
O IV] 1402	0.3::	...	...
C II] 2323	0.2::	...	...
C II 4267	...	...	...
C III] 1909	2.0	...	...
C IV 1549	6.6	...	...
[N I] 5200	...	...	...
[N II] 5755	...	...	0.04:
[N II] 6584	0.10	0.05	2.12
N III] 1750	...	...	...
N IV] 1485	2.9:	...	...
N V 1240	0.3::	...	...
[Ne III] 3869	0.98	0.66	1.59
[Ne IV] 2423	...	...	...
[Ne IV] 4725	...	...	...
[Ne V] 3426	...	...	...
[S II] 4069	0.006	...	...
[S II] 6717	0.077	...	0.292
[S II] 6731	0.099	...	0.248
[S III] 6312	0.018	0.015	0.019
[Ar III] 7136	0.147(2)	...	...
[Ar IV] 4711	0.047	0.065	...
[Ar IV] 4741	0.040	0.054	...
[Ar V] 7006	...	...	...
Δ Balmer /Hβ	...	...	...
c(Hβ)	0.23	0.22	0.29
t[O III]	1.21±0.08	1.31±0.08	1.4±0.3
t[N II]	...	...	1.15±0.12
t[O II]	...	...	...
t(Δ Balmer)	...	...	...
N_e[S II]	1.5±0.5	...	0.3±0.2
N_e[Ar IV]	1.8±0.5	1.6±0.5	...

(1) Θ is the angular distance from the central star
(2) Data from Kingsburgh & Barlow 1994.

temperature fluctuations (such as found in some of the planetary nebulae observed by Liu & Danziger 1993) occur. The possible existence of large temperature fluctuations in planetary nebulae, generally attributed to shocks, high density condensations or abundance inhomogeneities (Peimbert 1995, but see also Stasińska 1998) casts some doubt on the relevance of the interpretation of forbidden lines by usual techniques. For the three objects mentioned above, at least, we can be confident that the usual techniques should be valid.

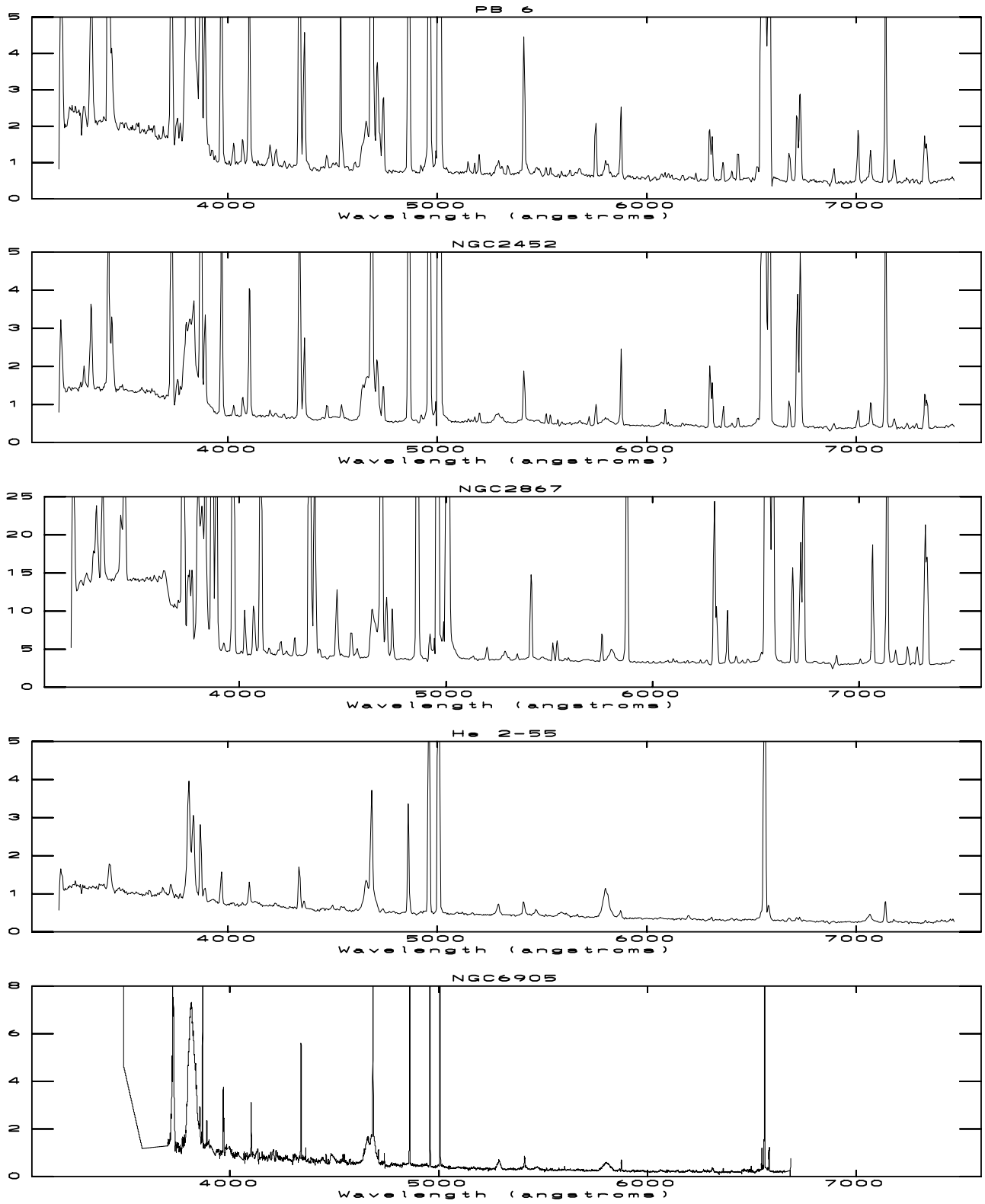

Fig. 2. Optical calibrated spectra of the central zones of the studied objects. From top to bottom we present: PB 6, NGC 2452, NGC 2867, He 2-55 and NGC 6905 (notice that the spectral resolution is much higher for the latter object). Fluxes are in units of 10^{-15} erg cm^{-2} s^{-1} Å^{-1}, except for NGC 6905 where the units are 10^{-14} erg cm^{-2} s^{-1} Å^{-1}. The stellar emission features are very intense in all of the objects. Nebular emission lines are much narrower and also very intense.

Table 3e. Dereddened fluxes for He 2-55.

	pos CS	pos1	pos2
$\Theta^{(1)}$	0”	4”	4”
extraction ap.	$2'' \times 7''$	$2'' \times 7''$	$2'' \times 7''$
He I 5876	0.043$^{(2)}$	0.046	0.034
He II 1640	7.04	...	...
He II 4686	1.20	0.998	0.998
[O I] 6300	0.006	0.005	0.002
[O II] 3727	0.229	0.195	0.147
[O II] 7325	...	...	...
O III] 1663	1.8:	...	...
[O III] 4363	0.095	0.121	0.098
[O III] 5007	8.13	9.07	8.11
O IV] 1402	...	...	...
C II] 2323	...	...	...
C II 4267	...	...	...
C III] 1909	2.6	...	...
C IV 1549	3.1$^{(2)}$	...	...
[N II] 5200	...	...	...
[N II] 5755	0.0028	0.002:	...
[N II] 6584	0.104	0.078	0.059
N III] 1750	0.78$^{(2)}$	...	...
N IV] 1485	0.3:	...	...
N V 1240	0.45$^{(2)}$	...	...
[Ne III] 3869	0.862	0.899	0.861
Ne IV] 2423	...	...	
[Ne IV] 4725	0.001:	0.001:	0.001:
[Ne V] 3426	0.021	...	...
[S II] 4069	...	0.023	0.030
[S II] 6717	0.016	0.032	0.018
[S II] 6731	0.015	0.025	0.017
[S III] 6312	0.016	0.023	0.016
[Ar III] 7136	0.119	0.156	0.133
[Ar IV] 4711	...	0.066	0.063
[Ar IV] 4741	0.045	0.041	0.046
Δ Balmer /Hβ	...	...	4.2-03
c(Hβ)	0.60	0.50	0.60
t[O III]	1.22$\pm$0.06	1.29$\pm$0.06	1.24$\pm$0.06
t[N II]	1.4$\pm$0.1	1.2$\pm$0.1	...
t[O II]	...	...	...
t(Δ Balmer)	...	...	1.2:
N_e[S II]	0.5$\pm$0.2	0.2$\pm$0.2	0.5$\pm$0.2
N_e[Ar IV]	...	0.1:	0.3$\pm$0.2

(1) Θ is the angular distance from the central star
(2) probable contamination with stellar emission

3. Photoionization modelling

3.1. The ionizing fluxes

The ionizing fluxes of the central stars have been obtained from models of expanding atmospheres for [WR] central stars, developed in Potsdam in the recent years. The model procedure, which accounts adequately for the extreme non-LTE situation and the velocity field, has been described in detail by, for instance, Hamann & Wessolowski (1990) and Hamann et al. (1994). The models are computed assuming a spherically symmetric, homogeneous and stationary outflow. The radiation transport is calculated in the co-moving frame and the solution, achieved by the accelerated lambda iteration (ALI), is consistent with the equation of statistical equilibrium. The basic parameters which can be derived by fitting the most important spectral features of a stellar wind are: the chemical composition, the terminal wind velocity, v_∞, the effective temperature, T_*, and a quantity termed the “transformed radius” defined as $R_t \sim R_*(v_\infty/\dot{M})^{2/3}$.

The main results of such an analysis for the objects in this work will be briefly described here. The reader interested in a more detailed description of the modelling procedure is referred to the paper by Koesterke & Hamann (1997b) where the authors present a detail analysis for the central stars of Sand 3, a [WC 3] type star (very similar to the objects studied here), and NGC 6751, a [WC 4] star.

Several individual models have been calculated for each of the program stars in order to match the shape and strength of the optical and, if *IUE* spectra were available, the *UV* emission lines. The most important lines considered are: C IV 4686, 5470 and 5805 Å, He II 4686, 4860 and 5412 Å, O V 5598 and O VI 5290 Å. The O VI blend at 3820 Å is not useful to constraint the model because the blend intensity is not well reproduced (in general, models for WCE stars predict a line twice weaker than observed). The reason for this failure is still unknown. The O V 5598 and O VI 5290 Å lines are very useful to determine ionization stratification of the stellar wind, which depends sensitively on the interplay of temperature and mass-loss rate. As one example the line fit for NGC 6905 is shown in Fig. 3 where the best fit (thick solid line) is presented with the alternative (cooler) model employed in the photoionization structure calculations (see Sect. 4). In this figure it is clear that both models fit well the He II and C IV lines, but the higher temperature model reproduces much better the highly ionized O V 5598 and O VI 5290 Å lines. Although the analysis produces a very sensitive fit and changes of about 2000 K in temperature do significantly alter the O V and O VI synthetic lines, the uncertainty of the temperature determination is definitely much larger due to systematic errors, as the fact of neglecting iron line-blanketing, possible inhomogeneities in the atmospheres and the assumption of a steady and symmetric outflow. In Table 1 are tabulated the best-fit values for T_* and R_t, as given by Koesterke & Hamann (1997a), for the stars in this work.

3.2. Fitting the overall photo-ionization structure

Photoionization models were constructed using the code PHOTO (Stasińska 1990) with the atomic data updated as described in Stasińska & Leitherer (1996). Spherical symmetry is assumed and the diffuse ionizing radiation field is treated with the outward-only approximation. A model is obtained by specifying the properties of the ionizing star, and the chemical composition and density structure of the nebula. It is computed

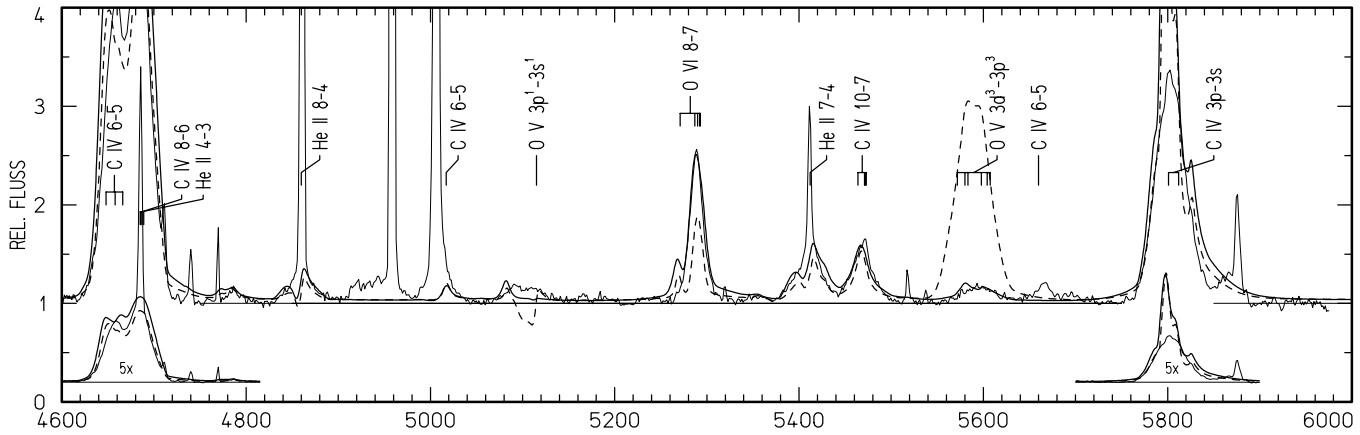

Fig. 3. Line fit of the central star of NGC 6905 in the optical. The best model atmosphere (T_*=141 kK, thick solid line) is shown together with the synthetic spectrum of the cooler model (128 kK, broken line) which is finally used for the photoionization structure of the nebula. Both models fit well, in strength and shape, the He II and C IV lines but the hotter model reproduces much better the ionization stratification of the highly ionized oxygen lines. The cooler model shows O V much stronger and O VI weaker than observed.

inside out, by adding successive layers until a specified property of the observed nebula is reproduced (or until the gas becomes neutral). Here, as explained below, this property is the observed [O III] 5007/[O II] 3727 ratio on the central line of sight, which then determines how much a given model is density bounded.

To further constrain the models, in addition to the relative line intensities, the following observational data were used: the dereddened stellar visual magnitudes, the total nebular fluxes in Hβ, the angular radii of the main body of the nebulae and their morphological appearance. The distance to the nebulae being uncertain, we constructed models where the nebulae were supposed to lie at 0.5, 1, 2, 4 and 8 kpc from the Sun.

For each object, we first used the best-fit model atmosphere and, for each assumed distance, the stellar luminosity required to produce the observed stellar visual magnitude was calculated. With this luminosity, we computed a constant density photoionization model using the density deduced from the [S II] lines. The reason for starting with a constant density model even for objects that are obviously inhomogeneous in structure is that constant density photoionization modelling is the easiest and most widespread approach for modelling planetary nebulae. It is therefore interesting to see how well can homogeneous models fit a large number of observational constrains. At this stage, the elemental abundances were those obtained by adding the ionic abundances derived from the optical observations.

As mentioned above, the models were first required to reproduce the observed [O III] 5007/[O II] 3727 ratio on the line of sight passing through the center of the nebula. Then, we examined whether the computed He II 4686/Hβ ratio on this line of sight was equal, within the errors, to the observed one, for any of the chosen distances. This is the strongest constraint imposed on our models, and it is essential in order to correct reasonably for the unseen high ionization stages when calculating nebular abundances. As an additional check, the [Ne V] 3426/[Ne III] 3869 line ratio was used. We also required the computed nebular angular radius and the total Hβ flux to be compatible with the observations. That is to say, total computed Hβ fluxes somewhat higher than observed are acceptable, taking into account possible leakage of ionizing photons in some directions, but, models predicting a total Hβ flux much lower than observed (by more than about 50%, accounting for the uncertainty in the correction for extinction) were not considered satisfactory.

For PB 6 and NGC 2452, this procedure failed to produce the large He II 4686/Hβ and the [Ne V] 3426/[Ne III] 3869 ratios observed, whatever distance was considered. To obtain a larger He II 4686/Hβ, at a given [O III] 5007/[O II] 3727 and using the same stellar atmosphere, one needs to consider a composite model with an inner zone of low density emitting a large part of the He II 4686 and [O III] 5007 lines, and an outer zone of density as given by the [S II] 6717/6731 line ratio, emitting most of the [O II] 3727 line. Such a density structure is actually a far better representation for all the nebulae. In direct images of the objects it is observed that, in particular, PB 6, NGC 2452, NGC 2867 and NGC 6905 present high density zones (knots), embedded in a more diffuse body (see Fig. 1).

Since the spatial information we have on our objects does not allow us to infer the 3D-density distribution in the PN envelopes, and since the photoionization code works in spherical symmetry anyway, we decided to explore the density parameter space in a schematic way. A 3×3 grid of two-density models (plus a homogeneous model) was built for each object, at each of the five distances listed above, in which we adopted the inner density as being 1/2, 1/4 and 1/8 of the outer density, and in each case, we started the increase in density at 3 different positions (determined by the amount of He II 4686 already emitted in the inner zone). We considered that this was a reasonable degree of sophistication of the models, and we then examined, for each object, which model provided the best fit to the conditions imposed above, including the morphological appearance. Note that, at this stage, the analysis is independent of the abundances of the elements (except for helium: a big change in the

helium abundances modifies the size of the model, but empirical helium abundances in our planetary nebulae are correct within 10% since there is no unseen neutral helium, and the temperature dependence of the hydrogen to helium emission lines ratio is very small).

None of our five PNe were satisfactorily reproduced with the grid calculated in such a way. In the cases of PB 6 and NGC 2452, the large [Ne V] 3426/[Ne III] 3869 line ratio observed, required a larger proportion of hard UV photons (energies > 100 eV), while for NGC 6905, NGC 2867, and He 2-55, this line ratio is much lower, indicating a smaller proportion.

Changes in the emergent UV photon distribution in the models of expanding atmospheres can be obtained by changing the effective temperature or the mass-loss rate. Variations of the mass-loss rate (or wind density) for the same effective temperature have not been considered in this paper, since Esteban et al. (1993) have found that changes in the mass-loss rate, for constant effective temperature, are a second order correction in the photoionization modelling procedure. We then computed a second series of models, using model atmospheres having more appropriate effective temperatures and whose predictions were still compatible with the observed stellar features.

3.3. Construction of the final models

From the second grid of models computed for each object, we selected the most acceptable one to derive ionization correction factors (*icf's*) and to correct for the unseen ions. The elemental abundances from the optical spectra passing through the central star were then estimated, and a new model was run with these abundances.

A final model was calculated, after some slight adjustments in the abundances, in order to reproduce the intensities of He I 5876, [N II] 6584, [Ne III] 3869, [O III] 5007, [S III] 6312 and [Ar III] 7136 on the central position. The final model parameters are listed in Table 4. The carbon abundances requires a special treatment, because of the large uncertainties expected in the carbon line intensities as mentioned in Sect. 2.3. We have thus calculated models with C/O ratios of 0.5, 1, 2 and 4 to explore the carbon abundance value. The relevance of the models with different C/O values will be considered in the next sections.

In some cases, models with different combinations of inner/outer zones from our grid were equally acceptable. Generally, they would lead to similar elemental abundances. Taking into account a possible error of 0.5 magnitude in the observed stellar magnitudes did not produce any significant difference in the results. For each object, the "best model" corresponds to a given distance of the PN, which turns out to be about 4 kpc in all the cases under study. However, the results, and especially the line ratios, are not very dependent on the assumed distance. Therefore, we caution against the use of this distance in order to argue on the absolute value of the stellar luminosity.

3.4. Graphical presentation of the models

To illustrate our modelling procedure, we present, in Figs. 4a-e, some of the models computed for the nebulae. Four diagrams are presented for each object showing the behavior of He II 4686/Hβ, [Ne V] 3426/[Ne III] 3869, the angular radius and the total nebular flux in Hβ, as a function of the assumed distance. In each diagram, the circles represent the constant-density models calculated with the initial stellar models (see Table 1). The squares represent our best composite models using the same star. The triangles represent our best composite models for our second choice of star, when needed. The observed values are indicated by horizontal lines.

In Figs. 5a-e, we present the line-of-sight intensity ratios computed in the final models (taking a distance of 4 kpc). as a function of the projected angular radius. Each panel corresponds to a different line ratio. The four curves plotted in each panel correspond to different C/O ratios (the curves being thicker for larger values of C/O). Observations for the different positions are represented by rectangles whose width is equal to the extraction aperture width, and whose height roughly represents the uncertainty in the line ratio. To compute the uncertainties, it was convenient to assume that, for all the objects except NGC 6905, one sigma error in the line intensity relative to Hβ is given by $0.06\ I(\lambda)^{0.8}$ in the optical range, and $0.5\ I(\lambda)^{0.85}$ in the *UV* range (after aperture and reddening corrections). For NGC 6905, we multiplied these values by two. The *UV* intensities marked with a colon in Tables 3a-e are more uncertain than given by the above formulae.

Note that the models are not expected to reproduce the observed C IV 1549 line intensity because this line is probably strongly contaminated by emission from the [WC] stars. Also, this line, as well as N V 1240, is a resonance line, and consequently subject to selective absorption by dust. The [O I] 6300 line is not plotted because we do not expect our models to reproduce its intensity well, since it is very much dependent on the likely presence of small scale condensations in the nebulae.

3.5. General comments on the models

On the whole, we find that our best fit models reproduce the optical line ratios of He, N, O, and Ne ions rather well (at least for the central line of sight), given the observational uncertainties and the many constraints considered. The tolerance for the *UV* lines, due to the observational uncertainties is so large that, generally, they do not provide useful constraints. High spatial resolution spectroscopy from the *UV* to the optical, with an instrument like STIS on the *HST*, is needed to solve the aperture problem, in order to use *UV* lines as reliable diagnostic tools in the study of nebulae.

Contrary to all previous photoionization modelling of observed nebulae, (except Esteban et al. 1993 and De Marco & Crowther 1998), our models do not have the ionizing radiation field as a true free parameter. It is of course much easier to fit ultraviolet lines when, in addition with the abundances and the

ionization structure, one can play with the heating rate provided by the ionizing star.

In two of our objects (PB 6 and NGC 6905), the Hβ fluxes computed in the models are significantly lower than the measured ones. Since, for each assumed distance, the stellar luminosity was adjusted to produce a visual magnitude equal to the observed one, this seems to indicate that the models of expanding atmospheres used for these objects may be predicting too few ionizing photons with respect to their emission in the V band.

This deficiency would get even worse when metal line-blanketing is accounted for. A new generation of non-LTE models, taking into account this process, have now become available (Werner & Dreizler 1993; Hillier 1997; Hillier & Miller 1998; Hubeny et al. 1998; Crowther et al. 1998b). In all the cases, the effect of Fe line blanketing is to depress the Lyman continuum flux. Most of these models concern massive WR stars of much lower temperatures than our objects, therefore they are not directly relevant to our objects. The models by Werner & Dreizler (1993) do concern relatively hot PN nuclei with effective temperatures of 90 000 K, but not [WR] nuclei. They show that line-blanketed ionizing fluxes would largely affect the highest ionized nebular line fluxes such as [Ne V] 3426 Å and He II 4686 Å relative to Hβ. This could be the case also for [WR] central stars. Until more realistic models for [WR] nuclei can be computed, the actual impact of line-blanketing on the ionizing fluxes for our nebulae cannot be estimated quantitatively.

As noted above, the distances to PNe cannot be well determined from photoionization modelling. We simply report that, for a distance of 4 kpc (where most of our best models lie), the total luminosities derived for the stars under study range between 700 and 3300 $L_{\odot}$. Such values are reasonable for PN nuclei, but obviously, more direct estimates of the distances are needed to discuss the position of these stars in a H-R diagram.

4. Elemental abundances

Because our models were forced to reproduce the [O II] /[O III], He II 4686/Hβ and [Ne III] /[Ne V] line ratios at best, they return a correct ionization structure (except for S and Ar, for which dielectronic recombination coefficients at nebular temperatures are not available). For those models which also reproduce the electron temperature sensitive ratios, the input abundances of the main elements (He, N, O and Ne) must correspond to the average abundances on the central line of sight.

The confidence interval for each abundance value has to be evaluated from a semi-empirical approach. To do this, we first computed the ionic abundances of He^{+}, He^{++}, O^{+}, O^{++}, C^{++}, N^{+}, Ne^{++}, S^{++}, Ar^{++} relative to H^{+} using standard methods with T_e(O III) for the doubly charged ions and T_e(N II) for the singly charged ones and the [S II] densities for all the ions. Then, the total abundances were derived using the *icf's* based on the best model for each object. For the lines of sight other than the central one, we did not use the models directly, since they do not reproduce the observed ionization structure well (the models being spherically symmetric while the nebulae may depart from such a geometry). For oxygen, we used the *icf's* of Kingsburgh & Barlow (1994), for nitrogen we adopted N/O=N^{+}/O^{+} and for neon, Ne/O=Ne^{++}/O^{++}, on each line of sight. For carbon, we used C/O=C^{++}/O^{++}. Indeed, our models show that such a procedure should be correct within 20% for all the nebulae of our study. For sulfur and argon, there is no simple formula, and we estimated the *icf's* from the models. However, as mentionned before, we do not expect the latter abundances to be accurate.

Table 4 presents the resulting abundances for all the studied objects. The uncertainties were estimated taking into account uncertainties in line intensity measurements and reddening corrections (which propagate into the electron temperature and density determinations as seen in Tables 3a-e), and *icf's*. For the C/O abundance ratio we present three values calculated from C III] 1909 / [O III] 5007, C II 4267/[O III] 5007 (using the effective recombination coefficients by Péquignot et al. 1991) and C III] 1909/O III] 1663 line intensity ratios. Discussions of the results are presented for each object separately.

5. Discussion of the objects

5.1. PB 6

This very high excitation nebula, ionized by a [WC 2] type star, has a diameter of $\sim 12''$ and shows a shell structure. It was observed at parallactic angle (P.A. 135°) and spectral data for three different positions were extracted: the central zone (including the star) and the zones at 5.″3 and 6.″6 at each side of the central star (in these positions the shell presents maximum emission). Special care was taken to extract the nebular lines in the central zone without contamination of the stellar emission lines. This can be done confidently because the nebular lines are much narrower than the stellar ones and can be easily deblended.

Our modelling procedure led to a reasonable model for this object, once we abandoned the original stellar model with T_*=140 kK and R_t=4.50 $R_{\odot}$, for a hotter one having T_*=158 kK and R_t=3.98 $R_{\odot}$. Several facts argue towards a slightly higher stellar temperature yet (or a harder ionizing radiation field): the spatial extension of the [Ne V] 3426 line is larger than predicted by the model and the predicted Hβ luminosity is lower than observed.

An interesting discrepancy between models and observations is the following. The C/O abundance ratio has to be larger than 2 in order to reproduce the observed C III] 1909 line intensity, but such a high C abundance would depress the electron temperature resulting in a [O III] 4363/5007 ratio lower than observed (see Fig. 5a). The C/O value derived from C III] 1909/[O III] 5007 line ratio plus *icf's* from the photoionization model is 2.6, but the uncertainty exceeds 30% principally due to the reddening correction and the aperture correction required to match the *UV* and optical spectra. From the C III] 1909/ O III] 1663 ratio we obtain C/O = 2.4±1.3. In this case, there is no aperture correction (both lines are observed in the same *IUE* spectrum), and the dependence of the derived C^{++}/O^{++} ratio on the adopted electron temperature is small, but the large uncertainty is mainly due to the low signal-to-noise in O III] 1663.

Table 4. Photoionization models and total abundances

	PB 6	NGC 2452	NGC 2867	NGC 6905	He 2-55
$T_*(\mathrm{kK}), R_t(\mathrm{R}_\odot)$	158, 3.98	158, 3.98	128, 5.20	128, 5.20	128, 5.20
$N_{\rm in}/N_{\rm out}$	1/8	1/4	1/4	1/8	1/4
$L(\mathrm{H}\beta)_{\rm in}/L(\mathrm{H}\beta)_{\rm out}$	0.6	0.9	0.8	0.9	0.6
He/H$^{(1)}$	0.170	0.127	0.110	0.108	0.130
O/H$^{(1)}$ (10^{-4})	2.9	3.5	3.9	3.1	3.6
N/O$^{(1)}$	1.38	0.80	0.28	0.32	0.28
C/O$^{(1)}$	...	...	...	...	...
Ne/O$^{(1)}$	0.31	0.23	0.21	0.22	0.19
S/O$^{(1)}$	0.080	0.057	0.038	0.110	0.050
Ar/O$^{(1)}$	0.013	0.014	0.005	0.028	0.011
	pos. 1	pos. 1	pos. 1	pos. 1	pos. 1
He/H	0.176±0.008	0.127±0.006	0.112±0.006	0.108±0.007	0.147$^{(2)}$
O/H (10^{-4})	3.2±0.5	4.2±0.6	4.3±0.6	3.7±0.7	3.4±0.5
N/O	1.3±0.2	0.6±0.1	0.27±0.05	0.37±0.07	0.35±0.06
C/O (1909/5007)	2.6±1.1	1.1±0.5	3.1±1.3	0.9±0.4	1.3±0.5
C/O (4267/5007)	7.3±1.8	3.9±1.6	4.2±1.1	...	5.5±1.4
C/O (1909/1663)	2.4±1.3	...	3.3±1.6	...	...
Ne/O	0.25±0.04	0.21±0.03	0.19±0.03	0.23±0.04	0.23±0.03
S/O	0.04±0.02	0.04±0.02	0.03±0.02	0.08±0.04	0.04±0.02
Ar/O	0.012±0.006	0.013±0.007	0.004±0.002	0.03±0.01	0.013±0.007
	pos.2	pos. 2	pos. 2	pos. 2	pos. 2
He/H	0.172±0.008	0.130±0.007	0.111±0.006	0.117±0.006	0.132±0.007
O/H (10^{-4})	3.3±0.5	5.6±1.1	3.3±0.5	3.9±0.7	3.6±0.5
N/O	1.4±0.2	0.7±0.1	0.32±0.06	0.29±0.05	0.29±0.05
C/O	...	...	...	...	...
Ne/O	0.24±0.04	0.26±0.04	0.20±0.03	0.18±0.03	0.21±0.04
S/O	0.03±0.02	0.04±0.02	0.03±0.01	0.08±0.04	0.05±0.03
Ar/O	0.011±0.06	0.013±0.007	0.006±0.003	...	0.016±0.008
	pos. 3	pos. 3	pos. 3	pos. 3	pos. 3
He/H	0.172±0.008	0.128±0.006	0.106±0.005	0.13±0.02	0.122±0.006
O/H (10^{-4})	3.6±0.7	5.0±1.0	3.8±0.6	3.6±1.1	4.2±0.6
N/O	1.4±0.2	0.7±0.1	0.27±0.05	0.30±0.06	0.27±0.05
C/O	...	...	...	...	...
Ne/O	0.24±0.04	0.26±0.04	0.22±0.03	0.30±0.07	0.22±0.04
S/O	0.03±0.02	0.04±0.02	0.03±0.01	0.05±0.03	0.04±0.02
Ar/O	0.010±0.005	0.012±0.006	0.008±0.004	...	0.015±0.008
		pos. 4			
He/H		0.122±0.006			
O/H (10^{-4})		6.2±1.2			
N/O		0.6±0.1			
C/O		...			
Ne/O		0.22±0.04			
S/O		0.04±0.02			
Ar/O		0.011±0.06			
		pos. 5			
He/H		0.128±0.006			
O/H (10^{-4})		6.9±1.4			
N/O		0.5±0.1			
C/O		...			
Ne/O		0.22±0.04			
S/O		0.04±0.02			
Ar/O		0.010±0.005			

$^{(1)}$ abundances for the model

$^{(2)}$ probable stellar contamination in the He I lines

We explored the possibility that the observed C III] 1909 line may be contaminated by the star. Indeed, *IUE* spectra of Population I WC stars do show the C III] 1909, 1923 and C IV 1549 lines in emission (Niedzielski & Rochowicz 1994). In the case

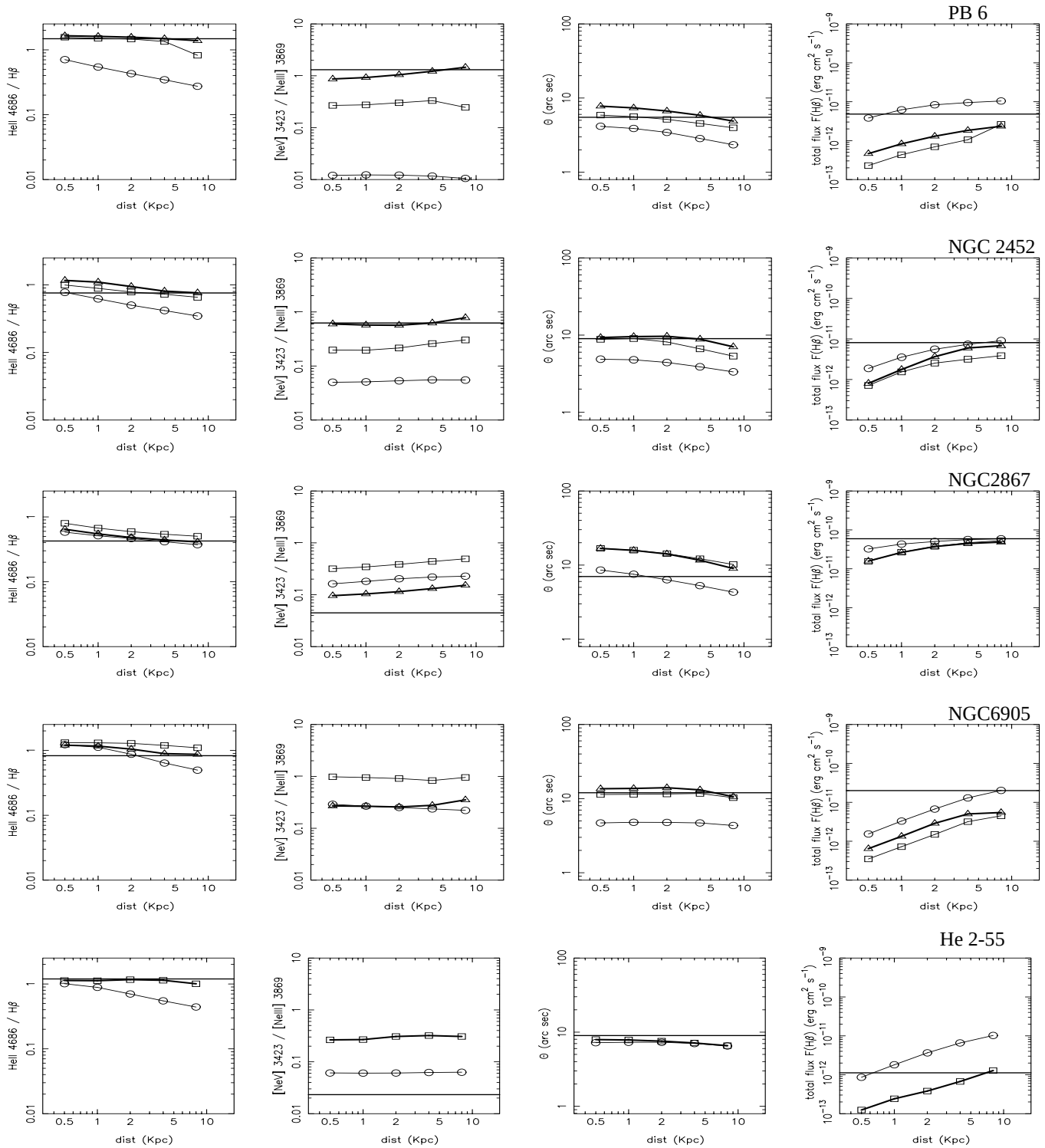

Fig. 4. Photoionization model predictions are shown. Four diagrams are presented for each nebula showing the behavior of He II 4686/Hβ, [Ne V] 3426/[Ne III] 3869, the angular radius and the total nebular flux in Hβ, as a function of the assumed distance. Circles represent the constant-density models calculated with the initial stellar atmosphere models (see Table 1). The squares represent the best two-density models using the same star. The triangles represent the best two-density models for our second choice of star (see Table 4). The observed values are indicated by horizontal lines.

of PB 6, however, our model atmospheres predict a negligible C III] 1909 equivalent width, therefore this explanation seems to be excluded.

The C/O ratio derived from the C II 4267/[O III] 5007 ratio is larger, by a factor of about 2.8, than the value from the C III] 1909 collisionally excited line. Such discrepancies be-

tween abundances derived from collisionally excited lines and recombination lines have been reported many times (see references in Stasińska 1998), and were originally attributed to low signal-to-noise data. Some authors have suggested that these discrepancies could be due to the presence of important temperature fluctuations in the ionized gas (see Peimbert et al. 1995 and references therein) and favor the recombination value. In the case of PB 6, our models show that adopting the C/O ratio derived from C II 4267 would result in an unacceptably low electron temperature. Clearly, PB 6 is one case where spectroscopy with an instrument like STIS would be necessary to provide better observational constraints.

The abundances derived for other elements are: O/H $\sim 3 \times 10^{-4}$, N/O$\sim$ 1.3 and He/H $\sim$ 0.17 (see Table 4). Although the C/O ratio is uncertain, it is likely to be larger than one. We find no evidence of a variation in abundance ratios across the nebula. The high C and N abundances in PB 6 are consistent with a scenario of C produced via the triple-α process, and being brought to the surface through third dredge-up (Forestini & Charbonnel 1997). The envelope was sufficiently hot at the base for envelope burning to occur, enhancing the N abundance. All this indicates that PB 6 has a progenitor with initial mass larger than about 2.8 $M_{\odot}$.

Our abundances for this object can be compared with values derived by previous authors. Kaler et al. (1991) derived 7.9×10^{-4}, which they found surprisingly high for an object having a large N/O. But their estimate is strongly weighted by their determination of the O^{+3} ionic abundance from O IV] 1402 line using the O^{++} electron temperature which overestimates the O^{+3} abundance by a factor of about 3.

Henry et al. (1996), from the same optical data, found O/H = 6.29×10^{-4}. Their procedure was to obtain a first guess for O/H using the classical *icf*, O/H=(O^+ + O^{++})/H^+ (He^+ + He^{++})/He^+, from Torres-Peimbert & Peimbert (1977), which overestimates the oxygen abundance when the He^{++} zone is large, as is the case in PB 6. This first estimate was then corrected by applying the same *icf* to a tailored photoionization model for PB 6. However, this model was only constrained by the O^{++}, O^+ and S^+ lines, and consequently probably underestimated the He^{++} zone. As a result, they obtained an O/H ratio much larger than ours.

Torres-Peimbert & Peimbert (1977) had found O/H= 4.2×10^{-4}, a value similar to ours, using their *icf* scheme with an observed He II 4686/Hβ ratio of 1.08 only, significantly smaller than the value reported by Kaler et al. (1991) or our value. It should be noticed that the low He II 4686/Hβ ratio reported by Torres-Peimbert & Peimbert (1977) was observed in 1975, while Kaler et al. (1991) reported observations made in 1985 and our data were obtained in 1994. This could indicate that a hardening of the stellar radiation field occured 10–20 years ago. Such important short-time variations in central stars of PNe have been reported for other objects such as the case of LMC-N66 (e.g., Peña et al. 1997b). Monitoring of the central star of PB 6 would be interesting to search for variations of its atmospheric properties.

5.2. NGC 2452

This is also a nebula ionized by a [WC 2] star. The nebular diameter is $\sim 19''$ and the gas appears very clumpy. We obtained spectra from the central zone and the four bright knots shown in Fig. 1.

Similarly to the case of PB 6, the very high ionization level of the gas led us to abandon the initial stellar model having T_*=141 kK and R_t=3.98 $R_{\odot}$ for a hotter stellar model with T_*=158 kK and R_t=3.98 $R_{\odot}$, with good results. Though, again, the same arguments would tend to favor a yet slightly harder radiation field in the Lyman continuum.

In this object, the model is able to reproduce at the same time the intensity of the observed C III]1909 line and the observed [O III] 4363/5007 line ratio when C/O is of the order of 1. On the other hand, a C/O ratio of 3.9$\pm$1.6 such as derived from the C II 4267 recombination line would no longer be compatible with the electron temperature observed.

The abundances found for He, N, O and Ne (see Table 4) are very similar to the ones determined by Kingsburgh & Barlow (1994) from their observations. NGC 2452 is a He-, N- and C-rich nebula, although it is not as extreme as PB 6. Regarding Ar and S, the disagreement with Kingsburgh & Barlow values is large (a factor of 3). This is not surprising, since, as mentioned before, empirical *icf's* for these ions are highly uncertain. Besides our models fail to reproduce the intensities of [Ar IV] and [Ar V] lines correctly.

Like in PB 6, the different zones investigated in NGC 2452 present the same chemical composition, within the uncertainties.

Although the present stages of the central stars in PB 6 and NGC 2452 appear very similar and the nebulae show very similar ionization degree, the abundances of helium, nitrogen and, possibly, carbon in NGC 2452 are significantly lower than in PB 6.

5.3. NGC 2867

This object, also excited by a [WC 2] type star, shows a knotty shell structure, with a diameter of about 25″. Two of the brightest knots, located at 4″ at each side of the central star in P.A. of 70°, were analyzed together with the central star position (see Fig. 1). The available *IUE* spectra of this object were recently studied in detail by Feibelman (1998), who classified the central star as an O VI type star.

Compared to PB 6 and NGC 2452, NGC 2867 presents a lower He II 4686/Hβ ratio and a much lower [Ne V] 3426 / [Ne III] 3869 ratio. To reproduce these values with our photoionization models, we had to replace the initial stellar model proposed by Koesterke & Hamann (1997a) (T_* = 141 kK, R_t = 3.98 $R_{\odot}$), for a cooler one with T_* = 128 kK, R_t = 5.20 $R_{\odot}$. Even this cooler model induces a predicted [Ne V]/[Ne III] ratio higher than observed (see Fig. 4), therefore, the star is probably still slightly cooler (or it produces less photons with energies above 100 eV). Note that, for this object, a homogeneous model can reproduce the line intensities and ionization struc-

ture reasonably well, but a composite model better represents the observed morphology of the nebula.

Here, similarly to the case of PB 6, we find a problem with the carbon lines, more severe this time. The observed [O III] 4363/5007 ratio tends to favor a moderate C/O ratio of 0.5 – 1, in conflict with the observed C III] 1909/[O III] 5007 line ratio which indicates a value of about 3. The C/O ratio derived from C III] 1909/O III] 1663 intensity ratio is also high, 3.3±1.6. As in PB 6, it is not expected that the central star contributes to the C III] 1909 emission, although it does so to the C IV 1549 emission. Therefore NGC 2867 is another interesting target for STIS observations. Note that the C/O abundance ratio derived from the C II 4267 recombination line is 4.2±1.1. If such a value represented the true C/O ratio, the observed [O III] 4363/5007 ratio would be even more discrepant.

Our computed O/H abundance ratio of $4.3 \pm 0.6 \times 10^{-4}$ is smaller by a factor of 1.4 than the value obtained by Kingsburgh & Barlow (1994) for the same object. The discrepancy is due to the large difference between their [O III] 5007/Hβ intensity ratio of about 17, and our value of 13.6, which is above our uncertainties. Our value is derived from several spectra with different exposure times trying to avoid saturation problems, therefore we are confident in our data. The abundances of nitrogen and helium in this nebula are not especially enhanced, and are similar in all the positions observed. Therefore from the point of view of chemical composition, NGC 2867 seems to be a normal disk PN.

5.4. NGC 6905

This nebula, ionized by a [WC 2–3] type star, shows a filamentary core of 24″ in diameter, and two faint conical lobes ending in 'ansae'. Three positions have been analyzed: the central zone around the central star (pos. 1), a knot at 5″ E from the central star (pos. 2), and the southern ansa located at 20″ from the central star (pos. 3).

NGC 6905 does not show any [Ne V] 3426 in emission (the upper limit estimated by Rowlands et al. (1993) is [Ne V] 3426/H$\beta < 0.05$). For this reason, in the modelling we had to replace the initial stellar model with T_* = 141 kK and R_t = 3.41 $R_\odot$, for a cooler one having T_* = 128 kK and R_t = 5.20 $R_\odot$, and even this cooler model predicts a too high [Ne V]/[Ne III] ratio (see Fig. 4).

Here, as in the case of NGC 2452, the carbon abundance derived from the C III] 1909 line induces an electron temperature that is compatible with the observed [O III] 4363/5007 ratio.

The chemical composition obtained for NGC 6905 shows no special He- or N-enrichment and is similar to that of NGC 2867. Again, we find no evidence for abundance variations among the different regions studied. In particular, the value derived for N/O is the same in the ansa as elsewhere.

The ansa, however, deserve more attention. Cuesta et al. (1992) have performed long slit spectroscopy of this nebula, together with high resolution spectroscopy centered on Hα. They noted an enhancement of [N II] 6584/Hβ in the southern ansa while [O III] 5007/Hβ kept a high level, and different kinematical properties. This led them to propose that the ansae were the result of a collimated stellar wind shock interacting with an outer halo. They also mentioned the possibility that the nitrogen abundance could be enhanced there. Our spectroscopic data for the ansa reveal important additional facts. The [O II] 3727 and [O I] 6300 lines are enhanced as well as [N II] 6584, the electron density is rather small, and the [O III] 4363/5007 ratio is marginally higher than in the main body of the nebula. That [O II] 3727 is enhanced similarly to [N II] 6584 excludes the possibility of N-enrichment. The presence of an intense [O I] 6300 line by itself is not sufficient to indicate the presence of shocks. Indeed, we have constructed photoionization models for the ansa that reproduce the observed intensities in all the low ionization lines, including [O I] 6300. The ionization parameter in the region of the ansa is small, and if there is enough matter there, the ansa will emit very strongly even in [O I] 6300. However the models hardly reproduce the very high [O III] 5007/Hβ observed and, the higher [O III] 4363/5007 ratio seen in the ansa argues in favor of a deposition of additional energy there. Therefore, our observations strengthen the picture proposed by Cuesta et al. (1992) of the ansae being the result of shock interaction, and the emission line spectrum is probably due to a combination of photoionization and shock heating. Because of this, the uncertainties in the ansa abundances are larger than the formal error bars given in Table 4. However, it seems likely that the chemical abundances, and specially the N/O ratio, are indeed the same as elsewhere.

Our derived O/H ratio is lower, by a factor of two, than the value given by Kingsburgh & Barlow (1994). This is principally due to the much smaller *icf* $\sim$ 2.1, predicted by our model, compared to the *icf* of 3.34 employed by these authors which heavily relies on the small He^+ abundance detected in this object, and is therefore quite uncertain. Other elemental abundances, relative to oxygen, are equal within the errors.

5.5. He 2-55

This nebula is ionized by a [WC 3] central star. It presents a diffuse shell of low surface brightness with an angular diameter of about 20″. In contrast with the previous nebulae analyzed, this object has a lower ionization degree and a much lower density. It was observed at parallactic angle (P.A. 135°) and three positions were analyzed: the central zone and two zones at both sides of the central star.

A priori, from Fig. 4, it seems that a homogeneous nebular model excited by the best fit model atmosphere, having T_* = 128 kK and R_t = 5.20 $R_\odot$ would appear satisfactory. But the distance predicted is of about 0.5 kpc, implying a stellar luminosity of 16 $L_\odot$ and a nebular mass of $5 \times 10^{-4}\ M_\odot$. Such low values are of course not acceptable, and we computed two-density models with the same star. It can be seen though, that such models predict a too high [Ne V] 3426/[Ne III] 3869 intensity ratio when the observed He II 4686/Hβ ratio is reproduced. Probably the star is cooler than assumed (or it emits less photons above 100 eV).

For this object, there is an acceptable solution for C III] 1909/Hβ with C/O $\sim$ 1, but it is not clear to what extent the C III] 1909 line is affected by stellar emission (Feibelman 1995). The O III] 1663 and N III] 1750 line intensities predicted by the models are below the observed ones by factors 5 to 10. However, the observed lines are very weak and noisy, moreover they are probably also be affected by blends from the star, so we do not consider that they provide useful constraints.

The abundances we derive for He, N, O and Ne are equal, within the errors, to those given by Kingsburgh & Barlow (1994). They are similar to the ones derived for NGC 2867 and NGC 6905, with the helium abundance being slightly larger by about 15% (the helium abundance in this object is better given by the values estimated in the off-center positions, since the He I 5876 line in the central position is probably contaminated by stellar emission). Again, we do not find evidence for any change in the chemical composition across the nebula.

6. Conclusion

We have obtained high signal-to-noise long slit spectra of five PNe with [WC 2–3] spectral type nuclei which enabled us to perform a detailed nebular analysis of these objects.

The stellar spectra were analyzed separately (Koesterke & Hamann 1997a), and models of expanding atmospheres have been constructed to reproduce the observed stellar features. We used the ionizing fluxes from these model atmospheres as an input for computing photoionization models of the nebulae. This is the first time that such self-consistent models are constructed for PNe ionized by early [WC] type stars. The observational constraints in our analysis are interestingly strong, due to the large number of ionic species observed.

The photoionization modelling was rather successful in reproducing at the same time the ionization structure and the electron temperature of the nebulae, although in some cases we had to replace the best-fit model atmospheres as proposed by Koesterke & Hamann (1997a) by models about 20 000 K hotter or cooler. The adopted models still reproduce, within the uncertainties, most of the observed stellar features.

For some objects, we had to release the classical constant-density assumption, in order to reproduce at the same time, the important intensity ratios He II 4686/Hβ, [Ne V] 3426/[Ne III] 3869 and [O III] 5007/[O II] 3727. Actually, the composite density models which we proposed are also in better agreement with the observed morphology of the studied nebulae.

In a couple of objects, we found that the Hβ fluxes predicted by models were lower than the observed ones. This led us to suspect that the models of expanding atmospheres employed could be slightly short of ionizing photons with respect to their emission in the V band.

The ionization structure predicted by our models is considered to be accurate for He, C, N, O and Ne ions, allowing thus to derive the abundances of these elements with good confidence. On the other hand, the models are not expected to reproduce the observed emission line ratios of sulfur and argon ions, since the atomic data are incomplete for these ions. Consequently, the abundances of these elements are not accurate.

Concerning the nature of the nebulae, we find that the five objects studied in this work, in spite of having central stars with very similar optical features, display very different morphologies, ionization degrees and abundance patterns. PB 6 is an extremely helium- nitrogen- and probably carbon-rich planetary nebula (a classical Type I PN), whose central star's progenitor was sufficiently massive to experience 2nd and 3rd dredge-up events, while NGC 2452 is also a N- and He-rich nebula, although not as extreme. These two objects show the highest ionization degree among the nebulae studied here and both required stellar atmosphere slightly hotter than those providing the best fit to the observed stellar features. NGC 2867, NGC 6905 and He 2-55 show a lower ionization degree than PB 6 and NGC 2452. They do not present He- or N-enrichment, showing N/O $\sim$ 0.3 and He/H $\sim$ 0.12. They could be classified as normal disk PNe. Their progenitors probably were not as massive as those of PB 6 and NGC 2452. Thus, clearly, post-AGB stars of quite different initial masses can pass through a [WC] stage with similar atmospheric parameters.

In none of the objects did we find significant abundance variations in N/O, Ne/O or He/O across the face of the nebula.

The only common fact for all the objects is that C/O $\geq$ 1, that is, all the nebulae show C-enrichment, probably due to the third dredge-up event. In this sense, the sample of galactic WRPNe studied here shows a behavior similar to that of the WRPNe in the Magellanic Clouds (Peña et al. 1997a). However, the last word on carbon abundances is not said. In PB 6 and NGC 2867, we found that the range of carbon abundances, compatible with the nebular temperature derived from the observed [O III] 4363/5007 line ratio, predicts C III] 1907/Hβ ratios below the value estimated from *IUE* observations. This is specially noticeable in NGC 2867, where the discrepancy is by a factor of 3, i.e., larger than the estimated uncertainties. It is not excluded that the error involved in the linking of nebular *IUE* and optical spectra may be much larger than estimated. Observations with an instrument like STIS on the *HST* would be extremely valuable to better fix the observational constraints.

The discrepancy mentioned above become much important if we adopt the C/O ratios derived from the recombination C II 4267 lines, which are larger by factors of 2 to 4. Our photoionization models show that such high carbon abundances would depress the electron temperatures to a level much lower than indicated by the observations. Therefore, we are inclined to think that the carbon abundances derived from optical recombination lines are not correct, and that this is not a consequence of low signal-to-noise data.

The high signal-to-noise optical spectroscopy presented here allowed us to investigate the possible existence of temperature fluctuations (Peimbert 1995) in our objects. If such fluctuations exist at a level of $t^2 = 0.02 - 0.04$, a Balmer-decrement temperature significantly smaller than the [O III]4363/5007 temperature should be found. This is not the case in the three nebulae for which our data allow a confident Balmer-decrement temperature determination.

Another important remark is the fact that the central stars, being of [WC] spectral type, present extremely H-deficient atmospheres and are presently ejecting He-burning products. According to Koesterke & Hamann (1997a) the chemical composition of the stellar winds consists of 60 to 70% of helium, 20% or more of carbon and about 10% of oxygen. This highly processed material has been ejected from the central star with mass loss rates near $10^{-6}\ M_{\odot}$/yr for more than 50 years (at least since the time of their discovery as [WR] stars). That is, the stellar wind should have accumulated more than $5 \times 10^{-5}\ M_{\odot}$ of He, C and O in the inner part of the nebulae. We did not find evidence for contamination by such a material in the central zones or in any of the knots studied. In this respect, our result is similar to the one by Esteban et al. (1992) for ring nebulae surrounding Population I WR stars. Much higher spatial resolution observations in both the optical and the *UV*, such as can be obtained with the *HST*, could provide more light on this subject.

Acknowledgements. We thank S. Górny for his assistance concerning the WRPN images. This work received partial support from CNRS-CONACyT/México agreement (grant E130-983) and DGAPA/UNAM (grant IN109696).

References

Acker, A., Marcout, J., Ochsenbein, F., Stenholm, B., Tylenda, R., 1992, The Strasbourg-ESO Catalogue of Galactic Planetary Nebulae
Balick, B., 1989, Planetary Nebulae, IAU Symp. 131, S. Torres-Peimbert (ed.), Kluwer, Reidel, 83
Crowther, P.A., Bohannan, B., Pasquali, A., 1998b, Properties of Hot, Luminous Stars, ASP Conference Series 131, I. Howarth (ed), p. 38
Crowther, P.A., De Marco, O., Barlow, M.J., 1998a, MNRAS, 296, 367
Cuesta, L., Phillips, J.P., Mampaso, A., 1992, A&A, 267, 199
De Marco, O., Crowther, P., 1998, MNRAS, 296, 419
Esteban, C., Vílchez, J.M., Smith, L.J., Clegg, R.E.S., 1992, A&A, 259, 629
Esteban, C., Smith, L.J., Vílchez, J.M., Clegg, R.E.S., 1993, A&A, 272, 299
Feibelman, W., 1995, ApJ, 449, L87
Feibelman, W., 1998, ApJSS, 114, 263
Forestini,M., Charbonnel, C., 1997, A&AS, 123, 241
Górny, S.K., Stasińska, G., 1995, A&A, 303, 893
Hamann, W.-R., 1997, Planetary Nebulae, IAU Symp. 180, Habing H., Lamers H. (eds.), Reidel, Kluwer, 91
Hamann, W.-R., Wessolowski, U., 1990, A&A, 227, 171
Hamann, W.-R., Wessolowski, U., Koesterke, L., 1994, A&A, 281, 184
Hamuy, M., Walker, A.R., Suntzeff, N.B., et al., 1992, PASP, 104, 533
Henry, R.B.C., Kwitter, K.B., Howard, J.W., 1996, ApJ, 458, 215
Hillier, J., 1997, WR Stars in the Framework of Stellar Evolution, 33$^{\rm rd}$ Liège Int. Astroph. Coll., L.M. Vreux et al. (eds.), 491
Hillier, D.J., Miller D.L., 1998, ApJ, 496, 407
Hubeny, I., Heap, S.R., Lanz, T., 1998, Properties of Hot, Luminous Stars, ASP Conference Series 131, I. Howarth (ed), 108
Hummer, D.G., Storey, P.J., 1987, MNRAS, 224, 609
Jacoby, G.H., Ford, H.C., 1983, ApJ, 266, 298
Johnson, H.M., 1981, ApJ 250, 590
Kaler, J.B., Shaw, R.A., Feibelman, W.A., Imhoff, C.L., 1991, PASP 103, 67
Kingsburgh R.L., Barlow M.J., 1994, MNRAS, 271, 257
Koesterke L., Hamann W.-R., 1997a, Planetary Nebulae, IAU Symp. 180, Habing H., Lamers H. (eds.), Reidel, Kluwer, 114
Koesterke L., Hamann W.-R., 1997b, A&A, 320, 91
Leuenhagen U., Hamann W.-R., Jeffery S., 1996, A&A, 312, 167L
Liu, X.W., Danziger, I.J., 1993, MNRAS, 263, 256
Méndez, R.H., Niemela, V., 1982, IAU Symp. 99, Wolf-Rayet stars:Observations, Physics, Evolution, de Loore C.W.H., Willis A.J. (eds.), Dordrecht, Reidel, 457
Meynet G., 1995, A&A, 298, 767
Niedzielski, A., Rochowicz, K., 1994, A&AS, 108, 669
Peimbert, M., 1995, The Analysis of Emission Lines, Williams R. E., Livio M. (eds.), Cambridge University Press, p. 165
Peimbert, M., Torres-Peimbert, S., Luridiana, V. 1995, Rev Mex Astron Astrof, 31, 131
Peña, M., Hamann, W.-R., Koesterke, L., et al., 1997b, ApJ, 491, 233
Peña, M., Ruiz, M.T., Torres-Peimbert, S., 1997a, A&A, 324, 674
Péquignot, D., Petitjean, P., Boisson, C., 1991, A&A, 251, 680
Rowlands, N., Houck, J.R., Skruttskie, M.F., Shure, M., 1993, PASP, 105, 1287
Seaton, M., 1979, MNRAS, 185, 57p
Schönberner, D., Blöcker, T., 1996, A&Sp Sci 245, 201
Schwarz, H.E., Corradi, R.L.M., Melnick, J., 1992, A&AS, 94, 399
Stasińska, G., 1990, A&AS, 83, 501
Stasińska, G., 1998, Abundance profiles: diagnostic tools for galaxy history, ASP Conf. Ser., ed. D. Friedli et al, in press
Stasińska, G., Leitherer, K., 1996, ApJSS, 107, 661
Torres-Peimbert, S., Peimbert, M., 1977, Rev Mex Astron Astrof, 2, 181
Tylenda R., Acker A., Stenholm B., 1993, A&AS, 102, 595
Werner K., Dreizler S., 1993, Acta Astronomica, 43, 321